Supporting Information

Cobalt-Based Non-Precious Metal Catalysts Derived from Metal–Organic Frameworks for High-Rate Hydrogenation of Carbon Dioxide

Xiaofei Lu,[†,#] Yang Liu,[‡,#] Yurong He,[§,#] Andrew N Kuhn,[†] Pei-Chieh Shih,[†] Cheng-Jun Sun,[∥] Xiaodong Wen,[*,§] Chuan Shi,[*,†,‡] and Hong Yang[*,†]

[†] Department of Chemical and Biomolecular Engineering, University of Illinois at Urbana Champaign, 600 South Mathews Avenue, Urbana, Illinois 61801, United States

[‡] State Key Laboratory of Fine Chemicals, College of Chemistry, Dalian University of Technology, Dalian, Liaoning 116024, P. R. China

[§] State Key Laboratory of Coal Conversion, Institute of Coal Chemistry, Chinese Academy of Sciences, P. O. Box 165, Taiyuan, Shanxi 030001, P. R. China

[∥] X-ray Science Division, Argonne National Laboratory, 9700 South Cass Avenue, Argonne, Illinois 60439, United States

* Corresponding authors: hy66@illinois.edu (HY), chuanshi@dlut.edu.cn (CS), and wxd@sxicc.ac.cn (XDW)

Methods Used in the Density Functional Theory Calculations. All the plane-wave-based density functional theory (DFT) calculations were performed with the Vienna Ab initio Simulation Package (VASP). The electron ion interaction was described with the projector augmented wave (PAW), potentials and the electron exchange and correlation energy was treated within the Perdew-Burke-Ernzerhof (PBE) function of generalized gradient approximations (GGA). The D3 dispersion correction was used to count for van de Waals interactions. Spin-polarization was included for iron systems to correctly account for the magnetic properties. The cut-off energy of 400 eV and electron smearing via a second-order Methfessel-Paxton technique with the width of 0.2 eV were employed to ensure accurate energies with errors less than 1 meV per atom. The sampling of the Brillouin zone was performed using a Monkhorst-Pack scheme. The convergence criteria for electronic self-consistent interactions and all forces were set to 10^{-4} eV and 0.03 eV/Å, respectively.

To determine the RWGS elementary reactions with the minimum barriers, transition states were located using the climbing image nudged elastic band (CI-NEB) method, and stretching frequencies were analyzed to characterize a transition state with single imaginary frequency along the reaction coordinate. To describe the thermodynamic and kinetic properties of the reactions, adsorption energy, reaction energy, and activation energy were calculated. The adsorption energy is defined as E_{ads} = E(adsorbates/slab) - [E(slab) + E(adsorbates)], where E(adsorbates/slab) is the total energy of the slab with adsorbates, E(slab) is the total energy of the corresponding bare slab, and E(adsorbates) is the total energy of free adsorbates. The lower (more negative) E_{ads} means the stronger adsorption and the desorption energy is $-E_{ads}$. The reaction energy is defined as $E_r = E_{FS} - E_{IS}$. The activation energy is calculated by $E_a = E_{TS} - E_{IS}$ where E_{IS}, E_{FS}, and E_{TS} are the energies of the corresponding initial state (IS), final state (FS), and transition state (TS), respectively.

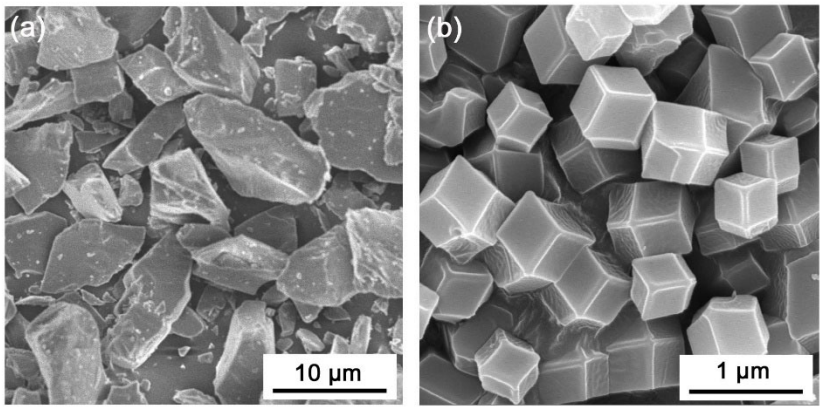

Figure S1. Representative SEM images of the MOF precursors: (a) $Co_3(BTC)_3 \cdot 12H_2O$ and (b) ZIF-67.

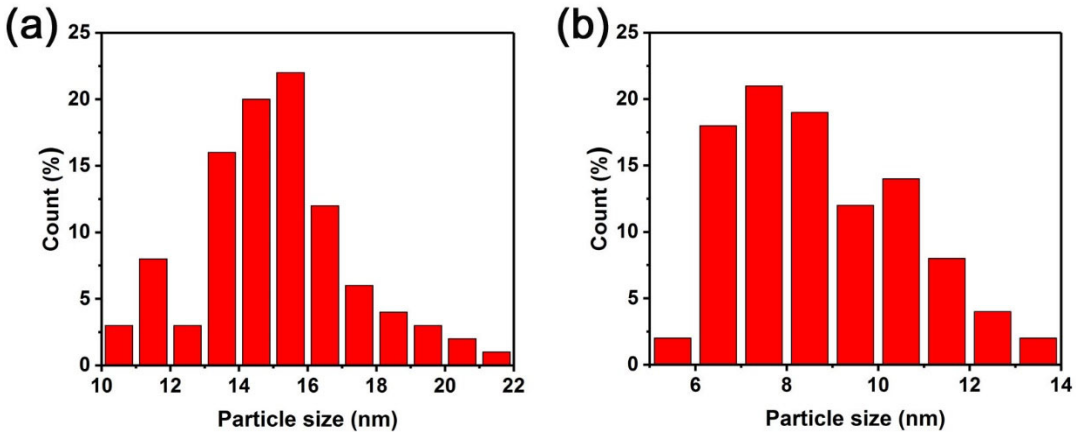

Figure S2. Size distribution analysis of Co particles for the (a) Co-C-700 and (b) Co-C-N-700 catalysts.

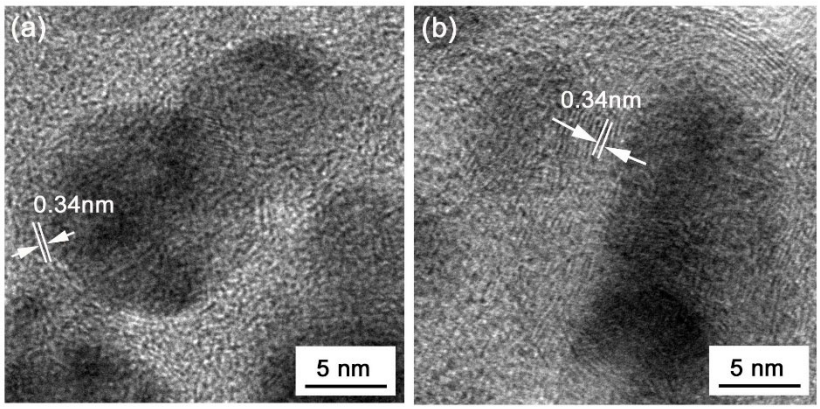

Figure S3. Representative TEM images of the (a) Co-C-N-700 and (b) Co-C-700 catalysts showing the lattice d-spacing of the carbon supports.

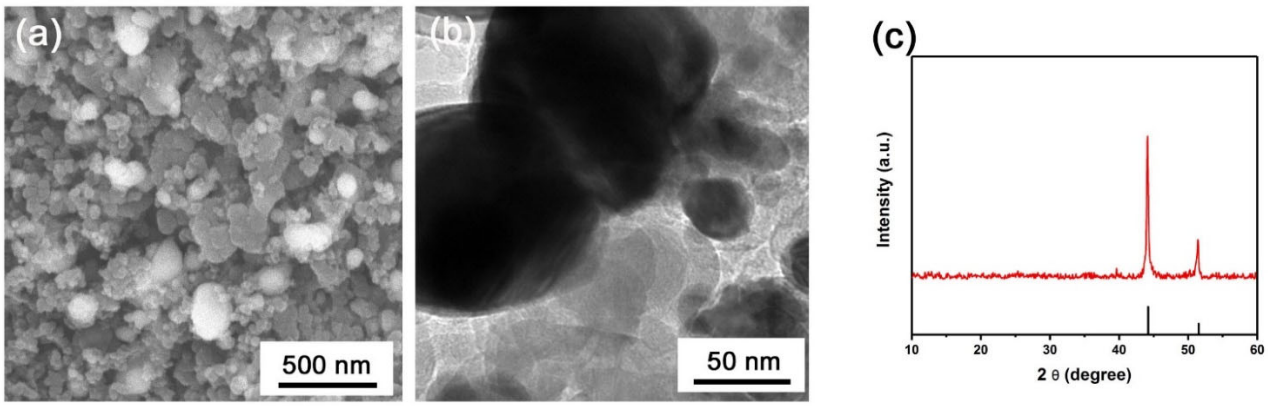

Figure S4. Representative (a) SEM, (b) TEM, and (c) power XRD pattern of the impregnated Co catalyst (im-Co-C-700, 63%).

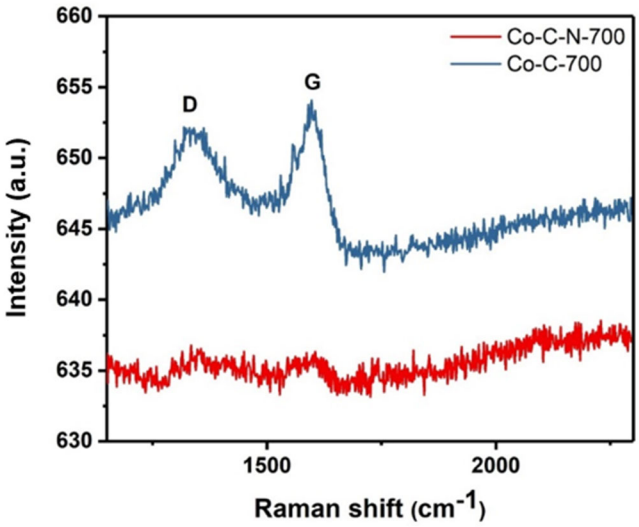

Figure S5. Raman spectra of the Co-C-700 and Co-C-N-700 catalysts, respectively.

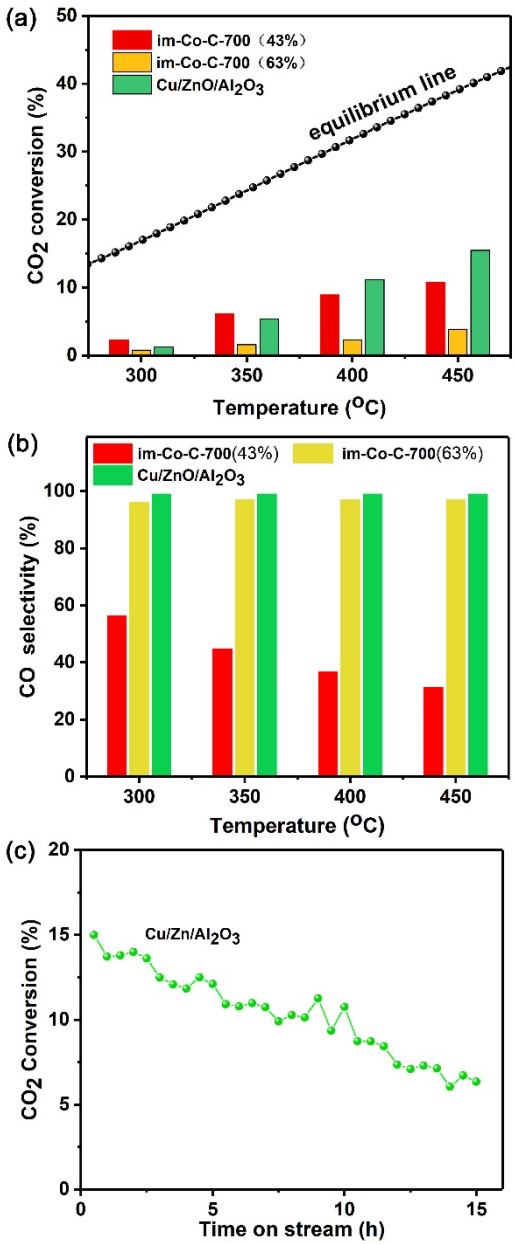

Figure S6. (a) CO_2 conversion and (b) CO selectivity of the reference catalysts at different reaction temperatures. (c) Stability study of $Cu/ZnO/Al_2O_3$ catalyst in the RWGS reaction at 450 °C. Feed conditions: CO_2:H_2 feed ratio =1:2; WHSV= 300,000 mL g^{-1} h^{-1}; and the pretreatment condition: H_2 (50 sccm) at 400 °C for 90 min.

.

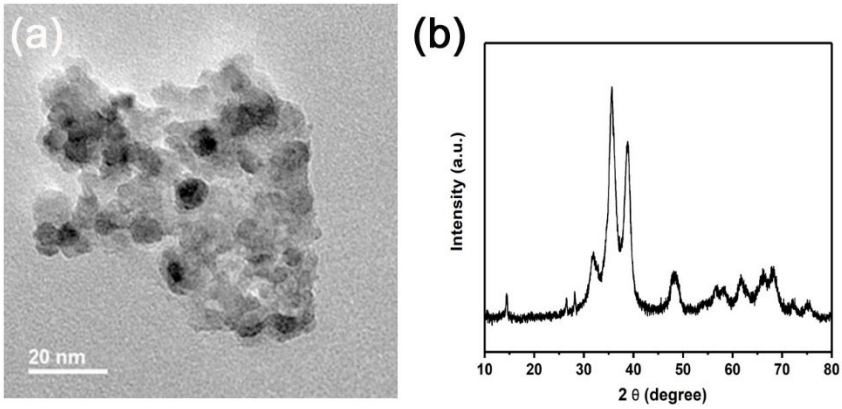

Figure S7. (a) TEM micrograph and (b) power XRD pattern of the reference Cu/ZnO/Al_2O_3 catalyst**.**

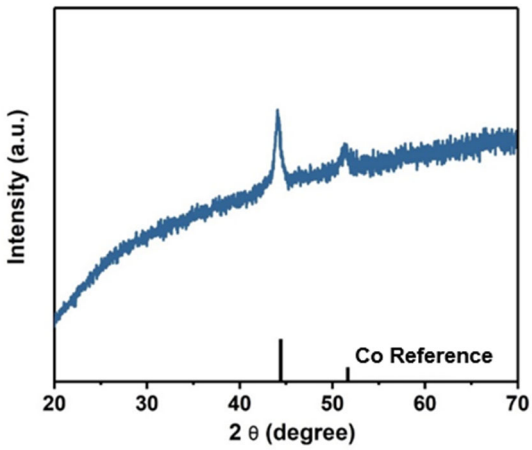

Figure S8. Power XRD pattern of the Co-C-N-700 catalyst after the reaction at 450 °C for 40 h.

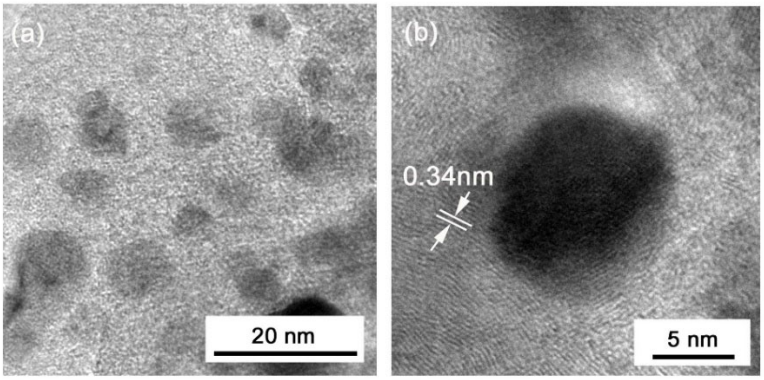

Figure S9. Representative (a) low and (b) high magnification TEM images of the Co-C-N-700 catalyst after the reaction at 450 °C for 40 h, showing the lattices of graphitic structure**s**.

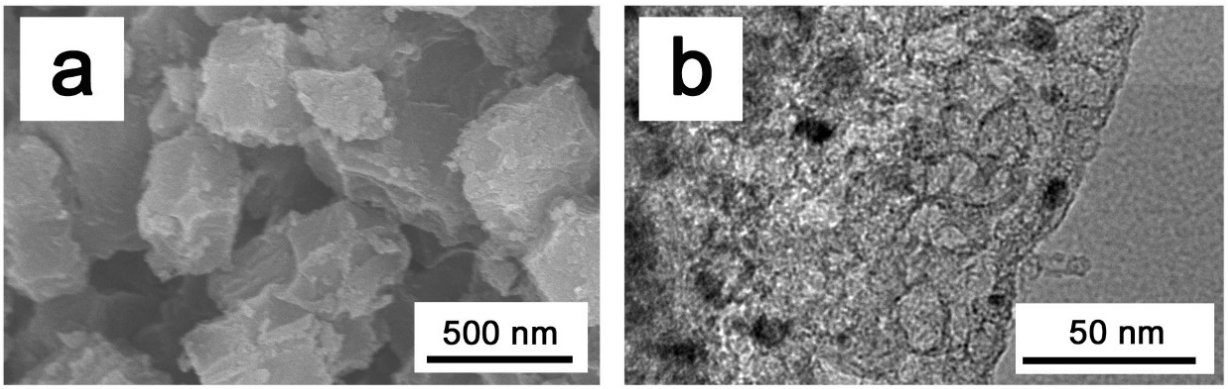

Figure S10. Representative (a) SEM and (b) TEM images of the Co-C-N-700 catalysts after acid etching.

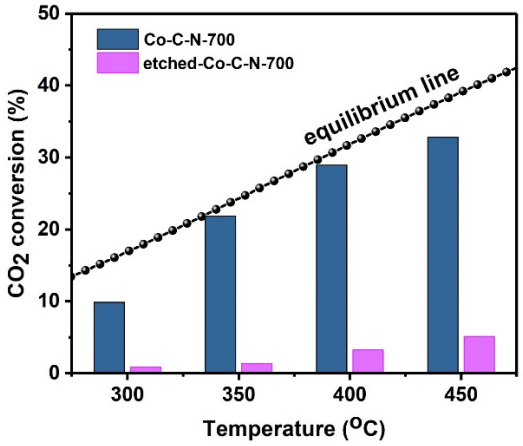

Figure S11. Comparison of catalytic performance between Co-C-N-700 and etched-Co-C-N-700 catalysts. The equilibrium line was drawn based on thermodynamic data from the HSC Chemistry software and database.

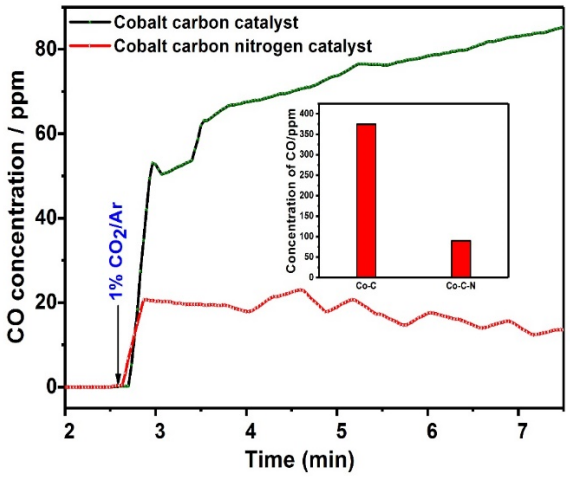

Figure S12. CO_2 dissociation at 400 °C on the Co-C-700 and Co-C-N-700 catalysts, determined by an IR analyzer. Conditions: Ar flow rate of 100 mL/min for the initial 2.5 min, and then 100 mL/min of a forming gas of 1% CO_2 in Ar.

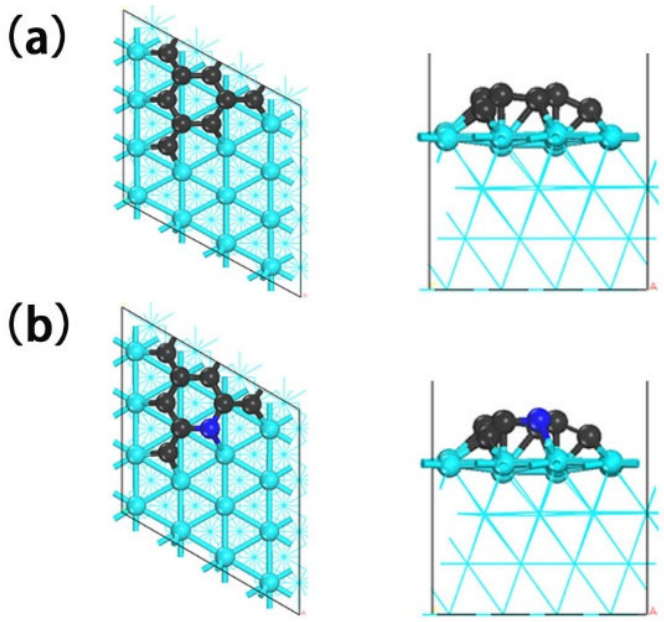

Figure S13. Illustrations of the top and side views of the surface of (a) Co-C-700 and (b) Co-C-N-700 catalysts. Color code: Co, cyan; C, black; and N, blue.

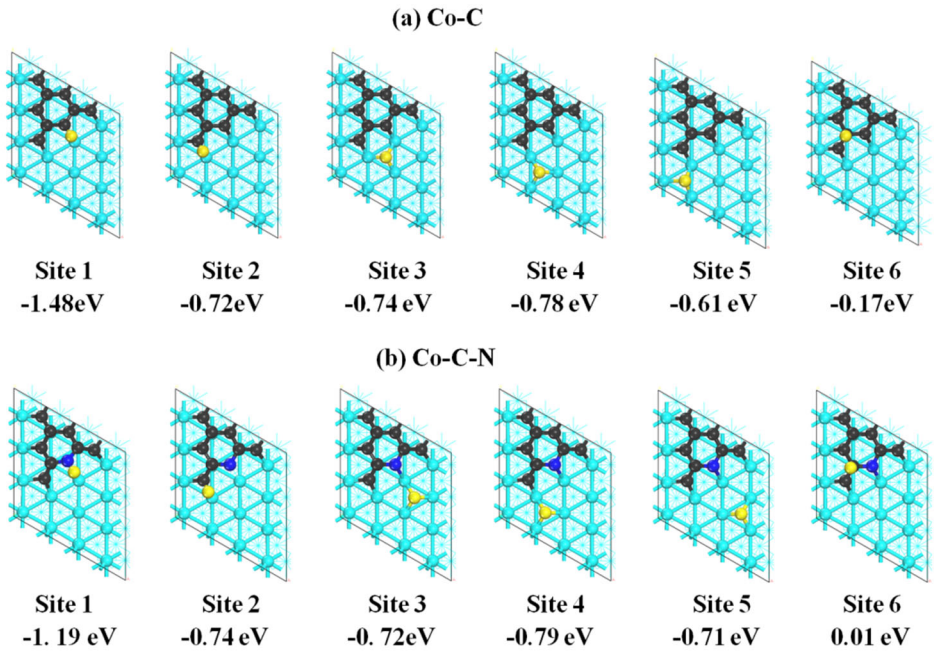

Figure S14. Illustrations of different configurations of H* adsorptions and their associated adsorption energy values on the (a) Co-C and (b) Co-C-N catalyst surfaces. Color code: Co, cyan; C, black; N, blue; and H, yellow.

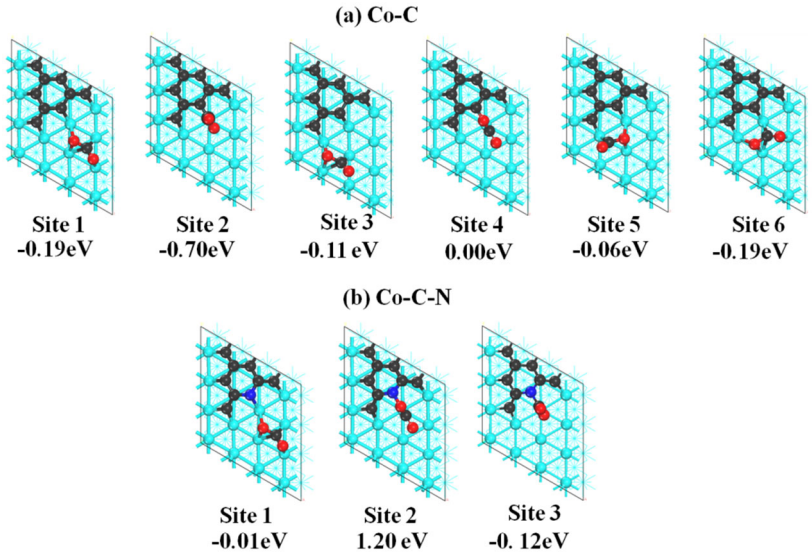

Figure S15. Illustrations of different configurations of CO_2* adsorptions and their associated adsorption energy values on the (a) Co-C and (b) Co-C-N catalyst surfaces. Color code: Co, cyan; C, black; N, blue**;** and O, red.

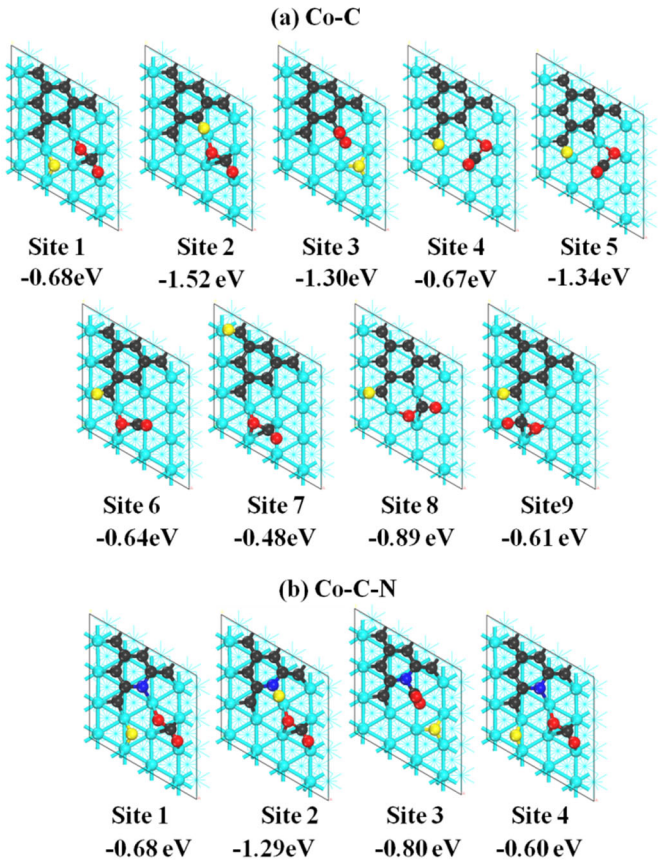

Figure S16. Illustrations of various configurations for H* and CO_2* co-adsorption on the (a) Co-C and (b) Co-C-N surfaces and their adsorption energy values. Color code: Co, cyan; C, black; N, blue; O, red; and H, yellow.

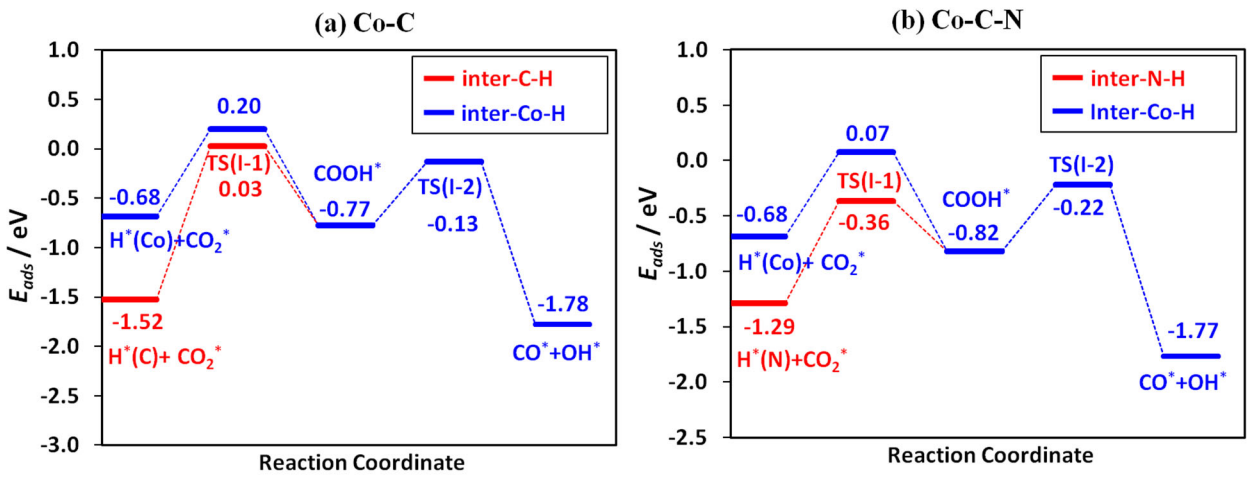

Figure S17. Potential energy diagrams for the formate mechanisms on the (a) Co-C-700 and (b) Co-C-N-700 surfaces. Blue lines: both CO_2* and H* are on Co atoms (Inter Co-H). Red lines: CO_2* is on Co atoms and H* is on an adjacent C (Inter-C-H) or N (Inter-N-H) atom for Co-C-700 and Co-C-N-700, respectively. The energy is given with respect to free CO_2 and H_2 gas molecules. If the value is greater than 0.0 eV in this pathway, the step has competing desorption reactions. For Co-C-700 (left), COOH* forms by H* adsorption on either Co or C because TS (I-1) has an E>0.0 eV. In contrast, COOH* forms via the Inter-N-H pathway on Co-C-N (right) as shown in Figure 7 of the main text.

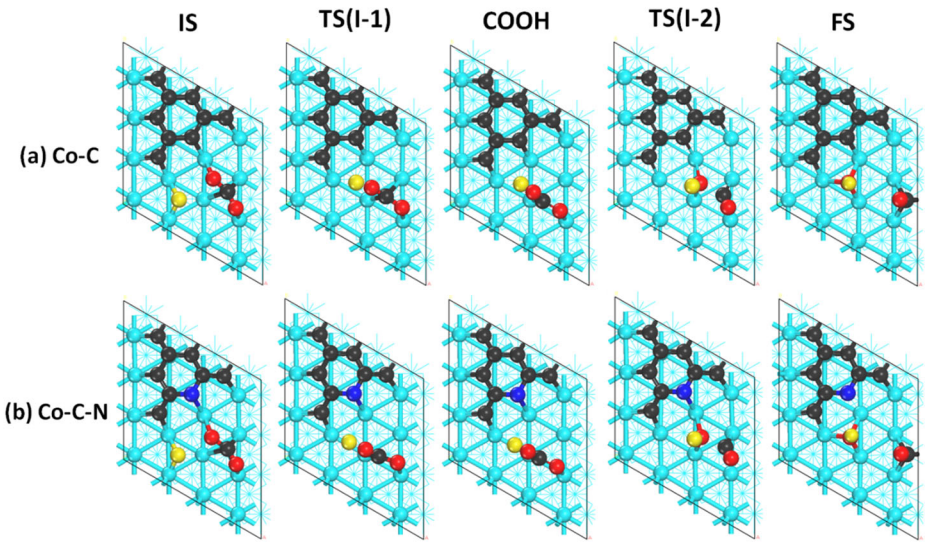

Figure S18. Schematic illustration for formate (COOH*) formation and decomposition from CO_2* and H* both adsorbed onto Co atoms for the (a) Co-C-700 and (b) Co-C-N-700 surfaces. The energies for these steps are represented as Inter-Co-H (blue line) in Figure S19. Color code: Co, cyan; C, black; N, blue; O, red; and H, yellow.

Table S1. Characterizations of catalysts tested in this work

Catalyst name	Elemental analysis (wt.%)				Property		
	N	C	Co	Other	S_{BET} ($m^2\ g^{-1}$)	Pore volume ($cm^3\ g^{-1}$)	Co particle size (nm)
Co-C-700	0	36.14	62.67	1.19	225	0.07	13-15
Co-C-N-700	5.17	48.73	43.24	2.86	415	0.13	7-9
Im-Co-C-700 (43%)	0	55.74	43	1.26	252	0.02	N/A
Im-Co-C-700 (63%)	0	36.1	62.6	1.3	263	0.01	>50

Table S2. Co dispersion and metallic surface area of the as-prepared Co-based catalysts*

Catalyst	Co-C-N-700	Co-C-700	Im-Co-C-700 (43%)	Im-Co-C-700 (63%)
Co loading (%)	43	63	43	63
Metal dispersion (%)	5.28	2.27	2.28	0.584
Metal surface area ($m^2\ g_{sample}^{-1}$)	10.72	9.22	9.26	1.18
Metal surface area ($m^2\ g_{Co}^{-1}$)	24.92	14.64	15.43	3.95

*: $\%\mathrm{D} = S_f \times \frac{V_{ads}}{V_g} \times \frac{m.w.}{\%_M} \times 100\%$, where S_f is the stoichiometry factor, V_{ads} is the volume adsorbed in $cm^3\ g^{-1}$, V_g is the molar volume of gas at STP and equal to 22.414 $m^3\ mol^{-1}$, *m.w.* is the molecular weight of the metal, in a.m.u., and $\%_M$ is the percentage of metal.

Table S3. Conversion of CO_2 and selectivity to CO for the RWGS reaction of the various selected catalysts reported in this work and in literature

Catalyst	Loading (wt%)	H_2:CO_2 ratio	Temperature (°C)	Pressure (MPa)	Rate ($\times 10^{-5}$ mol-CO_2/g_{cat}-s)	CO selectivity (%)	Reference
Co-C-700	N/A	2:1	300	0.1	6.03	88.5	This work
	N/A	2:1	400	0.1	30.1	86.0	This work
	N/A	2:1	450	0.1	35.7	89.7	This work
Co-C-N-700	N/A	2:1	300	0.1	12.2	83.6	This work
	N/A	2:1	400	0.1	35.9	88.7	This work
	N/A	2:1	450	0.1	40.7	90.7	This work
Cu/β-Mo_2C	1	2:1	600	0.1	47.7	99.2	1
Mo_2C	N/A	1:1	600	0.1	20	100	2
Co-Mo_2C	7.5	1:1	300	N/A	9.5	98	2
PtCo/TiO_2	1.75 Pt,1.5 Co	1:1	300	N/A	8.2	98.8	3
PtCo/CeO_2	1.75 Pt,1.5 Co	1:1	300	N/A	9.1	92.3	3
Ir/CeO_2	5.90	1:1	300	N/A	6.8	99	4
Cu/ZnO/Al_2O_3	36	2:1	500	0.1	10.53	100	1

1. Zhang, X.; Zhu, X.; Lin, L.; Yao, S.; Zhang, M.; Liu, X.; Wang, X.; Li, Y.-W.; Shi, C.; Ma, D., Highly Dispersed Copper over β-Mo_2C as an Efficient and Stable Catalyst for the Reverse Water Gas Shift (RWGS) Reaction, *ACS Catal.* **2016,** *7*, 912-918.

2. Porosoff, M. D.; Yang, X.; Boscoboinik, J. A.; Chen, J. G., Molybdenum Carbide as Alternative Catalysts to Precious Metals for Highly Selective Reduction of CO_2 to CO, *Angew. Chem. Int. Ed.* **2014,** *53*, 6705-6709.

3. Kattel, S.; Yu, W.; Yang, X.; Yan, B.; Huang, Y.; Wan, W.; Liu, P.; Chen, J. G., CO_2 Hydrogenation over Oxide-Supported PtCo Catalysts: The Role of the Oxide Support in Determining the Product Selectivity, *Angew. Chem. Int. Ed.* **2016,** *55*, 7968-7973.

4. Li, S.; Xu, Y.; Chen, Y.; Li, W.; Lin, L.; Li, M.; Deng, Y.; Wang, X.; Ge, B.; Yang, C., Tuning the Selectivity of Catalytic Carbon Dioxide Hydrogenation over Iridium/Cerium Oxide Catalysts with a Strong Metal-Support Interaction, *Angew. Chem. Int. Ed.* **2017,** *56*, 10761-10765.